

Surface modes in plasmonic Bragg fibers with negative average permittivity

HANYING DENG,¹ YIHANG CHEN,^{1,7} NICOLAE C. PANOIU,² BORIS A. MALOMED,^{3,4} AND FANGWEI YE^{5,6,8}

¹*School of Physics and Telecommunication Engineering, South China Normal University, Guangzhou 510006, China*

²*Department of Electronic and Electrical Engineering, University College London, Torrington Place, London WC1E7JE, United Kingdom*

³*Department of Physical Electronics, School of Electrical Engineering, Faculty of Engineering, Tel Aviv University, Tel Aviv 69978, Israel*

⁴*ITMO University, St. Petersburg 197101, Russia*

⁵*School of Physics and Astronomy, Shanghai Jiao Tong University, Shanghai 200240, China*

⁶*Department of Physics, Zhejiang Normal University, Jinhua 321004, China*

⁷*yhchen@scnu.edu.cn*

⁸*fangweiye@sjtu.edu.cn*

Abstract: We investigate surface modes in plasmonic Bragg fibers composed of nanostructured coaxial cylindrical metal-dielectric multilayers. We demonstrate that the existence of surface modes is determined by the sign of the spatially averaged permittivity of the plasmonic Bragg fiber, $\bar{\epsilon}$. Specifically, localized surface modes occur at the interface between the cylindrical core with $\bar{\epsilon} < 0$ and the outermost uniform dielectric medium, which is similar to the topologically protected plasmonic surface modes at the interface between two different one-dimensional planar metal-dielectric lattices with opposite signs of the averaged permittivity. Moreover, when increasing the number of dielectric-metal rings, the propagation constant of surface modes with different azimuthal mode numbers is approaching that of surface plasmon polaritons formed at the corresponding planar metal/dielectric interface. Robustness of such surface modes of plasmonic Bragg fibers is demonstrated too.

© 2022 Optical Society of America under the terms of the [OSA Open Access Publishing Agreement](#)

OCIS codes: (240.6680) Surface plasmons; (240.6648) Surface dynamics; (310.6628) Subwavelength structures, nanostructures; (350.4238) Nanophotonics and photonic crystals.

References and links

1. C. Poli, M. Bellec, U. Kuhl, F. Mortessagne, and H. Schomerus, "Selective enhancement of topologically induced interface states in a dielectric resonator chain," *Nat. Commun.* **6**, 6710 (2015).
2. Q. Cheng, Y. Pan, Q. Wang, T. Li, and S. Zhu, "Topologically protected interface mode in plasmonic waveguide arrays," *Laser Photon. Rev.* **9**(4), 392–398 (2015).
3. L. Lu, J. D. Joannopoulos, and M. Soljacic, "Topological photonics," *Nat. Photonics* **8**(11), 821–829 (2014).
4. S. Ke, B. Wang, H. Long, K. Wang, and P. Lu, "Topological edge modes in non-Hermitian plasmonic waveguide arrays," *Opt. Express* **25**(10), 11132–11143 (2017).
5. W. Su, J. R. Schrieffer, and A. J. Heeger, "Solitons in polyacetylene," *Phys. Rev. Lett.* **42**(25), 1698–1701 (1979).
6. H. Schomerus, "Topologically protected midgap states in complex photonic lattices," *Opt. Lett.* **38**(11), 1912–1914 (2013).
7. A. P. Slobozhanyuk, A. N. Poddubny, A. E. Miroshnichenko, P. A. Belov, and Y. S. Kivshar, "Subwavelength topological edge states in optically resonant dielectric structures," *Phys. Rev. Lett.* **114**(12), 123901 (2015).
8. I. S. Sinev, I. S. Mukhin, A. P. Slobozhanyuk, A. N. Poddubny, A. E. Miroshnichenko, A. K. Samusev, and Y. S. Kivshar, "Mapping plasmonic topological states at the nanoscale," *Nanoscale* **7**(28), 11904–11908 (2015).
9. L. Ge, L. Wang, M. Xiao, W. Wen, and C. T. Chan and D Han, "Topological edge modes in multilayer graphene systems," *Opt. Express* **23**(17), 21585–21595 (2015).
10. N. Malkova, I. Hromada, Ivan, X. Wang, G. Bryant, and Z. Chen, "Observation of optical Shockley-like surface states in photonic superlattices," *Opt. Lett.* **34**(11), 1633–1635 (2009).
11. M. Xiao, Z. Q. Zhang, and C. T. Chan, "Surface impedance and bulk band geometric phases in one-dimensional systems," *Phys. Rev. X* **4**(2), 130–136 (2014).

12. H. Deng, X. Chen, M. Xiao, N. C. Panoiu, and F. Ye, "Topological surface plasmons in superlattices with changing sign of the average permittivity," *Opt. Lett.* **41**(18), 4281–4284 (2016).
 13. J. Zak, "Berry's phase for energy bands in solids," *Phys. Rev. Lett.* **62**(23), 2747–2750 (2016).
 14. P. B. Johnson and R.-W. Christy, "Optical constants of the noble metals," *Phys. Rev. B* **6**(12), 4370–4379 (1972).
 15. P. Yen, A. Yariv, and E. Marom, "Theory of Bragg fiber," *J. Opt. Soc. Am.* **68**(9), 1196–1201 (1978).
 16. J. Scheuer and B. Malomed, "Annular gap solitons in Kerr media with circular gratings," *Phys. Rev. A* **75**(6), 063805 (2007).
-

1. Introduction

Surface modes induced by nontrivial topological mechanisms have recently drawn much attention in optics. Thanks to the topological protection, topological surface modes are intrinsically robust against structural perturbations [1–4]. A variety of optical systems supporting such surface modes have been proposed and demonstrated. The simplest example is analogous to the celebrated Su-Schrieffer-Heeger (SSH) model for polyacetylene [5], in which a chain of sites with alternating coupling constants exhibits two topologically distinct phases, and topologically protected interfacial modes exist at their interface. The photonic realization of the SSH model was demonstrated in dimerized dielectric waveguides [6], dielectric nanoparticles [7], and metallic nanodisks [8], as well as in graphene plasmonic waveguide arrays [9]. These structures, which implement the SSH model in photonics, are discrete one, as concerns the arrangement of their optical elements.

Topological surface modes can also be realized in one-dimensional (1D) continuous periodic systems [10–12]. In particular, the Zak phase, which is a special kind of the Berry phase defined for photonic bands of 1D systems, characterizes topological properties of such periodic systems [13]. Interestingly, it was found that the Zak phase of plasmonic superlattices, composed of alternating metallic and dielectric layers, is determined by the sign of the spatially averaged value of their permittivity [12]. Topologically protected plasmonic surface modes exist at the interface between two plasmonic lattices with opposite signs of the average permittivity, and these modes may be regarded as a generalization of conventional surface plasmonic polaritons (SPPs) occurring at the interface between dielectric and metallic materials. This means that for 1D plasmonic periodic systems the spatial average of the permittivity, which has a more intuitive physical meaning, acts as an alternative to the Zak phase in characterizing topological properties of the structure – namely, in defining the existence of topological surface modes. This raises an important question: can the sign of the average permittivity also determine the existence of plasmonic surface modes in metallic-dielectric structures, beyond the 1D case, such as in plasmonic Bragg fibers composed of coaxial cylindrical metal-dielectric multilayers?

In this paper, we consider a plasmonic Bragg fiber composed of coaxial cylindrical dielectric-metal multilayers and investigate physical properties of localized surface modes in such fibers by performing the mode analysis and direct beam-propagation simulations. We find that, similarly to the case of topological surface modes in planar metal-dielectric multilayers, surface modes exist at the interface between the core of the plasmonic Bragg fiber with a negative average permittivity and the outermost uniform dielectric medium. We also find that, with the increase of number of dielectric-metal rings of the plasmonic Bragg fiber, the propagation constant of all the modes, including the fundamental and higher-order ones, approaches that of surface plasmon polaritons formed at the planar interface between the metal and dielectric media. Finally, using direct numerical simulations, the surface modes of plasmonic Bragg fibers are found to be robust against structural disorder. The paper is organized as follows. In the next section we introduce the theoretical model which is used to describe optical properties of our structure. Then, in Sec. 3, we present and discuss the main results of our study. Finally, we summarize the results in Sec. 4.

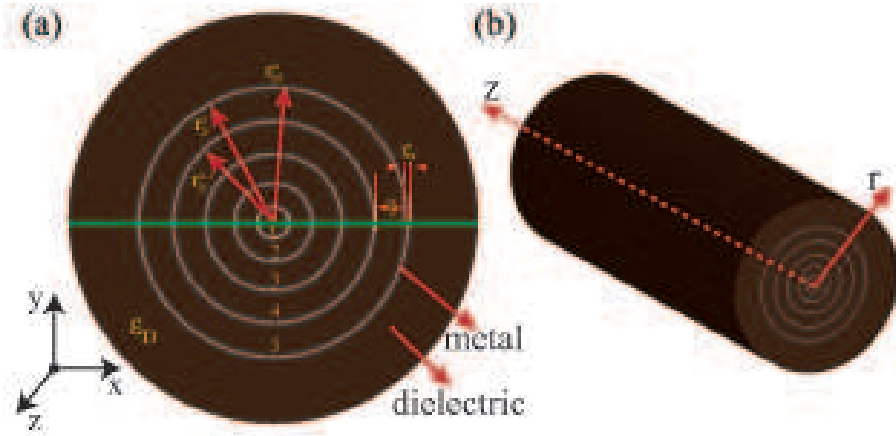


Fig. 1. (a) The cross-section of a plasmonic Bragg fiber composed of alternating coaxial metal-dielectric cylindrical shells. (b) A schematic structure of the plasmonic Bragg fiber.

2. The theoretical model and transfer-matrix formalism

The plasmonic Bragg fiber considered in this study is built as a series of coaxial metal-dielectric cylindrical shells, as schematically shown in Fig. 1. The electromagnetic field is assumed to propagate along the common axis of the cylindrical shells, z . To make the analysis more specific, we assume that the metallic and dielectric layers are made of silver and silicon, respectively. The complex permittivity of the metal (silver) can be calculated by using the Drude model [14], $\epsilon_M = 1 - \omega_p^2 / [\omega(\omega + i\nu)]$, with plasma and damping frequencies being $\omega_p = 13.7 \times 10^{15} \text{ rad s}^{-1}$ and $\nu = 2.7 \times 10^{14} \text{ rad s}^{-1}$, respectively. Note that the effect of interband transitions can be added to the Drude permittivity without qualitatively changing main conclusions of our analysis. The permittivity of the dielectric (silicon) is $\epsilon_D = 12.25$. The thickness of the metal layer is fixed to $t_M = 25 \text{ nm}$.

In order to be possible to use the operating wavelength to conveniently tune the average permittivity of the plasmonic Bragg fiber, $\bar{\epsilon}$, from being negative, passing through zero, to positive values, we assume that, at $\lambda = 1550 \text{ nm}$ ($\epsilon_M = -125.39$), the average permittivity of each metal-dielectric ring pair is tuned to zero; this of course also means that the average permittivity of the whole Bragg structure is zero. As we are concerned with TM-polarized waves and $\lambda \gg t_M, t_D$, this leads to the following expression at the corresponding wavelength:

$$\bar{\epsilon}_n = \frac{\epsilon_D S_D^n + \epsilon_M S_M^n}{S_D^n + S_M^n} = 0, \quad n = 1, 2, 3, \dots \quad (1)$$

where $S_M^n = \pi [(r_M^n)^2 - (r_M^n - t_M)^2]$ and $S_D^n = \pi [(r_M^n + t_D^n)^2 - (r_M^n)^2]$ are the cross-sectional areas of the n th metallic and dielectric cylindrical shells, respectively. r_M^n and t_D^n are the inner radius of the n th metallic cylindrical shell and the thickness of the n th dielectric cylindrical shell, respectively. As the thickness of the metallic shell is assumed to be fixed, thus the values for the series of the dielectric shells, t_D^n , can be obtained from Eq. (1).

Thus, thanks to the strong dispersion of the metallic permittivity, the average permittivity of such a plasmonic Bragg fiber,

$$\bar{\epsilon} = \frac{\sum_n (\epsilon_D S_D^n + \epsilon_M S_M^n)}{\sum_n (S_D^n + S_M^n)} = \frac{\sum_n \bar{\epsilon}_n (S_D^n + S_M^n)}{\sum_n (S_D^n + S_M^n)}, \quad (2)$$

can be shifted from negative to positive values by simply changing the operational wavelength. In our structure, the outermost layer is a homogeneous dielectric (silicon), whose thickness does

not have to satisfy $\bar{\epsilon}_n = 0$. Since the imaginary part of the permittivity of the metal is very small as compared to its real part ($\epsilon_M = -125.39 - 2.84i$), the influence of the metal loss on the results are found to be negligible. Nevertheless, in the following analysis we have taken into account this small imaginary part, unless otherwise stated.

The electromagnetic field in the plasmonic Bragg fiber can be calculated by employing the transfer-matrix method. Thus, the z -component of the electric and magnetic fields in the n th dielectric layer, which are a solution of the Maxwell equations expressed in cylindrical coordinates (r, θ, z) , can be written in the following form [15]:

$$\begin{aligned} E_z(r, \theta, z) &= [A_D^n I_m(k_D r) + B_D^n K_m(k_D r)] \cos(m\theta) e^{i\beta_m z}, \\ H_z(r, \theta, z) &= [C_D^n I_m(k_D r) + D_D^n K_m(k_D r)] \sin(m\theta) e^{i\beta_m z}, \end{aligned} \quad (3)$$

where $k_D = [\beta_m^2 - (\omega/c)^2 \epsilon_D]^{1/2}$ and, in the n th metallic layer, the fields are

$$\begin{aligned} E_z(r, \theta, z) &= [A_M^n I_m(k_M r) + B_M^n K_m(k_M r)] \cos(m\theta) e^{i\beta_m z}, \\ H_z(r, \theta, z) &= [C_M^n I_m(k_M r) + D_M^n K_m(k_M r)] \sin(m\theta) e^{i\beta_m z}, \end{aligned} \quad (4)$$

where $k_M \equiv [\beta_m^2 - (\omega/c)^2 \epsilon_M]^{1/2}$, I_m and K_m are the modified Bessel functions of the first and the second kind, respectively, β_m is the propagation constant, m is the azimuthal mode number which defines the order of the mode, ω is the angular frequency, and c is the speed of light in vacuum. Moreover, A_M^n , B_M^n , C_M^n , and D_M^n (A_D^n , B_D^n , C_D^n , and D_D^n) are modal amplitude coefficients within the n th metallic (dielectric) layers.

The transverse components of the fields can be expressed in terms of E_z and H_z using the following relations:

$$E_r = \frac{i\beta_m}{\omega^2 \mu \epsilon - \beta_m^2} \left(\frac{\partial E_z}{\partial r} + \frac{\omega \mu}{\beta_m} \frac{\partial H_z}{r \partial \theta} \right), \quad (5)$$

$$E_\theta = \frac{i\beta_m}{\omega^2 \mu \epsilon - \beta_m^2} \left(\frac{\partial E_z}{r \partial \theta} - \frac{\omega \mu}{\beta_m} \frac{\partial H_z}{\partial r} \right), \quad (6)$$

$$H_r = \frac{i\beta_m}{\omega^2 \mu \epsilon - \beta_m^2} \left(\frac{\partial H_z}{\partial r} - \frac{\omega \epsilon}{\beta_m} \frac{\partial E_z}{r \partial \theta} \right), \quad (7)$$

$$H_\theta = \frac{i\beta_m}{\omega^2 \mu \epsilon - \beta_m^2} \left(\frac{\partial H_z}{r \partial \theta} + \frac{\omega \epsilon}{\beta_m} \frac{\partial E_z}{\partial r} \right), \quad (8)$$

where $\mu = \mu_0$ is the magnetic permeability of vacuum.

Once the electromagnetic field in the n th dielectric layer is known, one can easily find the field in the n th metallic layer by applying the boundary conditions at the interface between the n th dielectric and metallic layers. The continuity of the tangential field components E_z , H_z , E_θ , and H_θ yields:

$$M_M(\rho) \begin{pmatrix} A_M^n \\ B_M^n \\ C_M^n \\ D_M^n \end{pmatrix} = M_D(\rho) \begin{pmatrix} A_D^n \\ B_D^n \\ C_D^n \\ D_D^n \end{pmatrix}, \quad (9)$$

with matrices

$$M_M(\rho) = \begin{pmatrix} I_m(\varrho_M) & K_m(\varrho_M) & 0 & 0 \\ \frac{\omega \epsilon_0 \epsilon_M}{\varrho_M} I'_m(\varrho_M) & \frac{\omega \epsilon_0 \epsilon_M}{\varrho_M} K'_m(\varrho_M) & \frac{m\rho}{\varrho_M^2} I_m(\varrho_M) & \frac{m\rho}{\varrho_M^2} K_m(\varrho_M) \\ 0 & 0 & I_m(\varrho_M) & K_m(\varrho_M) \\ \frac{m\rho}{\varrho_M^2} I_m(\varrho_M) & \frac{m\rho}{\varrho_M^2} K_m(\varrho_M) & \frac{\omega \mu_0 \mu_M}{\varrho_M} I'_m(\varrho_M) & \frac{\omega \mu_0 \mu_M}{\varrho_M} K'_m(\varrho_M) \end{pmatrix} \quad (10)$$

and

$$M_D(\rho) = \begin{pmatrix} I_m(\varrho_D) & K_m(\varrho_D) & 0 & 0 \\ \frac{\omega \varepsilon_0 \varepsilon_D}{\varrho_D} I'_m(\varrho_D) & \frac{\omega \varepsilon_0 \varepsilon_D}{\varrho_D} K'_m(\varrho_D) & \frac{m\rho}{\varrho_D^2} I_m(\varrho_D) & \frac{m\rho}{\varrho_D^2} K_m(\varrho_D) \\ 0 & 0 & I_m(\varrho_D) & K_m(\varrho_D) \\ \frac{m\rho}{\varrho_D^2} I_m(\varrho_D) & \frac{m\rho}{\varrho_D^2} K_m(\varrho_D) & \frac{\omega \mu_0 \mu_D}{\varrho_D} I'_m(\varrho_D) & \frac{\omega \mu_0 \mu_D}{\varrho_D} K'_m(\varrho_D) \end{pmatrix} \quad (11)$$

Here, $\rho = r_D^n$ is the inner radius of the n th dielectric cylindrical shell, and $\varrho_{M,D} = k_{M,D}\rho$. Moreover, Eq. (9) can be rewritten as:

$$\begin{pmatrix} A_M^n \\ B_M^n \\ C_M^n \\ D_M^n \end{pmatrix} = M_M^{-1}(\rho) M_D(\rho) \begin{pmatrix} A_D^n \\ B_D^n \\ C_D^n \\ D_D^n \end{pmatrix}. \quad (12)$$

Similarly, knowing coefficients of the electromagnetic fields in the n th metallic layer, one can determine their counterparts in the $(n+1)$ th dielectric layer by using the following matrix relation:

$$\begin{pmatrix} A_D^{n+1} \\ B_D^{n+1} \\ C_D^{n+1} \\ D_D^{n+1} \end{pmatrix} = M_D^{-1}(\rho') M_M(\rho') \begin{pmatrix} A_M^n \\ B_M^n \\ C_M^n \\ D_M^n \end{pmatrix}, \quad (13)$$

where $\rho' = r_M^n$ is the outer radius of the n th metallic cylindrical shell.

Equations (12) and (13) can be used iteratively to relate the amplitude coefficients in the first dielectric layer, i.e., A_D^1 , B_D^1 , C_D^1 , and D_D^1 , to their counterparts in the outermost dielectric layer, i.e., A_D^{n+1} , B_D^{n+1} , C_D^{n+1} , and D_D^{n+1} . The final result of this operation can be written as:

$$\begin{pmatrix} A_D^{n+1} \\ B_D^{n+1} \\ C_D^{n+1} \\ D_D^{n+1} \end{pmatrix} = M_D^{-1}(r_M^n) M_M(r_M^n) \cdots M_M^{-1}(r_D^1) M_D(r_D^1) \begin{pmatrix} A_D^1 \\ B_D^1 \\ C_D^1 \\ D_D^1 \end{pmatrix} = \begin{pmatrix} t_{11} & t_{12} & t_{13} & t_{14} \\ t_{21} & t_{22} & t_{23} & t_{24} \\ t_{31} & t_{32} & t_{33} & t_{34} \\ t_{41} & t_{42} & t_{43} & t_{44} \end{pmatrix} \begin{pmatrix} A_D^1 \\ B_D^1 \\ C_D^1 \\ D_D^1 \end{pmatrix}. \quad (14)$$

Two additional boundary conditions should be considered to determine the electromagnetic field in the plasmonic Bragg fiber. First, the fields in the first metallic layer must be finite, while K_m has a singularity at $r = 0$. This requires that $B_D^1 = D_D^1 = 0$. Second, the amplitude of the electromagnetic waves in the outermost dielectric layer (the cover) should be finite. This requires that $A_D^{n+1} = C_D^{n+1} = 0$, since I_m is infinite at $r \rightarrow \infty$. Thus Eq. (14) can be written as:

$$\begin{aligned} A_D^{n+1} &= t_{11} A_D^1 + t_{13} C_D^1 = 0, \\ C_D^{n+1} &= t_{31} A_D^1 + t_{33} C_D^1 = 0, \end{aligned} \quad (15)$$

which, in turn, may be expressed as

$$\begin{pmatrix} t_{11} & t_{13} \\ t_{31} & t_{33} \end{pmatrix} \begin{pmatrix} A_D^1 \\ C_D^1 \end{pmatrix} = 0. \quad (16)$$

In order for Eq. (16) to have non-trivial solutions, the determinant of the matrix must be zero, which gives:

$$\frac{t_{11}}{t_{31}} = \frac{t_{13}}{t_{33}}. \quad (17)$$

Once the structure of the plasmonic Bragg fiber structure is chosen and the frequency is fixed, Eq. (17) only depends on β_m . Therefore, the solution of Eq. (17) gives us the propagation constant of any optical mode of the fiber. After finding the value of β_m , one can determine values of A_D^1 and C_D^1 from Eq. (16). Subsequently, by combining this result with Eqs. (12) and (13), one can calculate the electromagnetic field in any layer of the plasmonic Bragg fiber.

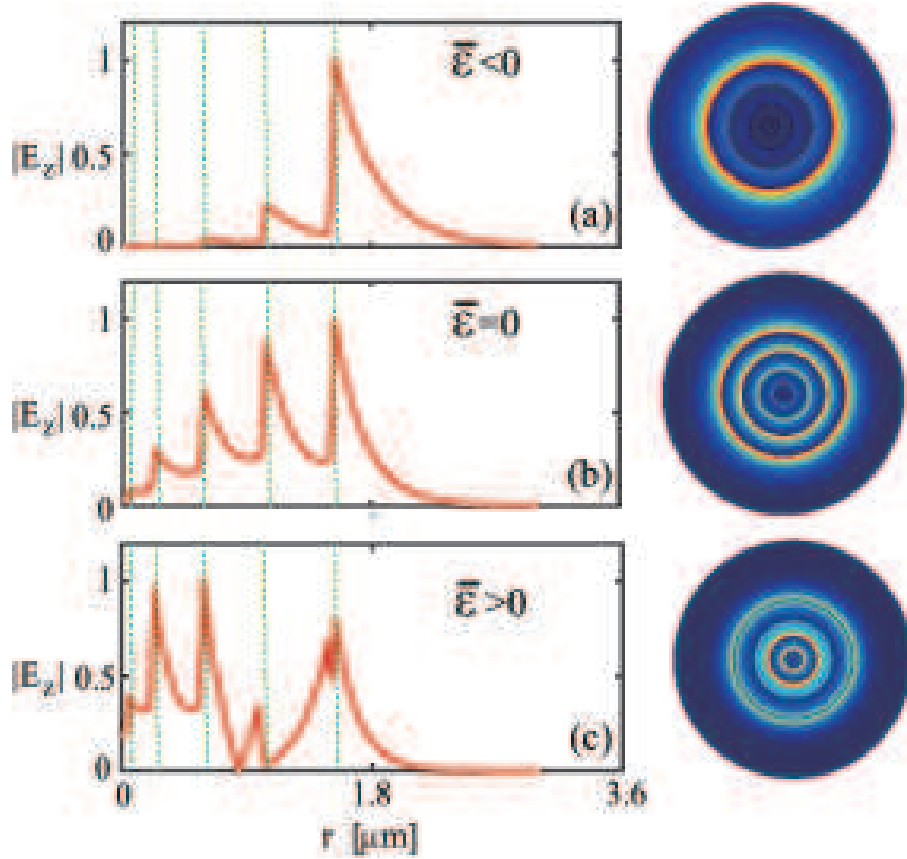


Fig. 2. The left (right) panel shows $|E_z|$ profiles of the fundamental mode of the plasmonic Bragg fiber with (a) $\bar{\epsilon} < 0$, (b) $\bar{\epsilon} = 0$, and (c) $\bar{\epsilon} > 0$, obtained by using the transfer-matrix method (COMSOL simulations). In all panels, the plasmonic Bragg fiber consists of five metal-dielectric ring units with $t_M = 25$ nm and $\epsilon_D = 12.25$. The average permittivities corresponding to the operational wavelength are: (a) $\bar{\epsilon} = -11.4 + 0.72i$ at $\lambda = 2.2$ μm , $\epsilon_M = -253.5 + 8.124i$; (b) $\bar{\epsilon} = 0$ at $\lambda = 1.55$ μm , $\epsilon_M = -125.39 + 2.84i$; (c) $\bar{\epsilon} = 2.2 + 0.1825i$ at $\lambda = 1.39$ μm , $\epsilon_M = -100.66 + 2.05i$. The green dashed lines indicate the interfaces between the metallic and dielectric layers.

3. Numerical results and discussion

We now employ the transfer-matrix formalism to calculate the field distribution in the plasmonic Bragg fibers and investigate the existence of localized surface states. First, we consider a plasmonic Bragg fiber composed of five dielectric-metal rings and surrounded by a homogeneous dielectric cladding with permittivity $\epsilon_D = 12.25$, as per Fig. 1. As discussed in the preceding section, the spatially averaged permittivity of such a plasmonic Bragg fiber can be tuned simply by varying the operational wavelength. Figure 2 shows the electric-field distribution of the fundamental mode, namely the mode with $m = 0$, of the plasmonic Bragg fiber, determined for the cases in which $\bar{\epsilon} < 0$, $\bar{\epsilon} = 0$, and $\bar{\epsilon} > 0$. These calculations were performed using both the transfer-matrix method and COMSOL simulations, an excellent agreement between the two approaches being observed. Similarly to the case of topological surface modes existing at the interface between two planar plasmonic superlattices with opposite signs of the averaged permittivity, these calculations reveal that, if the sign of the averaged permittivity of the plas-

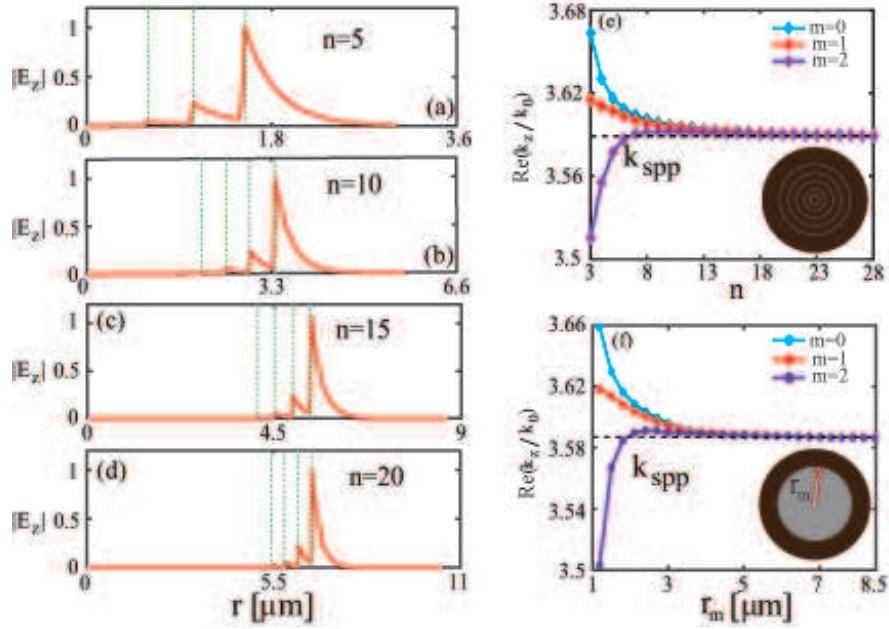


Fig. 3. (a), (b), (c), (d) Profiles of the electric field, $|E_z|$, of the surface modes located at the interface between a plasmonic Bragg fiber with $\bar{\epsilon} < 0$ and a uniform dielectric medium with $\epsilon_D = 12.25$. From top to bottom panels, the number of metal-dielectric rings, n , of the plasmonic Bragg fiber increases. (e) The dependence of the effective mode index of the plasmonic surface modes with $m = 0, 1, 2$, on the the number of the metal-dielectric rings. The black dashed line denotes the propagation constant of the SPPs at the corresponding planar metallic-dielectric interface. (f) The same as in (e) but with the plasmonic Bragg fiber replaced by a homogeneous metallic cylinder with the same radius. The green dashed lines indicate the interfaces between the metallic and dielectric layers.

monic Bragg fiber is negative, localized surface modes always exist at the interface between the plasmonic Bragg fiber and the outermost uniform dielectric medium, as shown in Fig. 2(a). On the other hand, no localized modes appear at the interface between the outermost uniform dielectric medium and the plasmonic Bragg fiber with $\bar{\epsilon} = 0$ and $\bar{\epsilon} > 0$, as shown in Figs. 2(b) and 2(c), respectively.

The condition for the existence of a localized surface state in the plasmonic Bragg fiber can be related to the formation of surface plasmon polaritons (SPPs) at the interface between two homogeneous and isotropic media. It is well known that SPPs exist only if the permittivities of the two media have opposite signs. As is illustrated in Figs. 3(a) through 3(d), indeed, the field profile of the surface modes resembles that of SPPs, with an additional feature represented by the field oscillations inside the plasmonic Bragg fiber. The similarity between conventional SPPs and surface modes in plasmonic Bragg fibers is also illustrated in Fig. 3(e), where we present the dependence of the propagation constant of the fundamental ($m = 0$) and higher-order ($m = 1, 2$) surface modes on the size of the plasmonic Bragg fiber. We note that, with the increase of the number of dielectric-metallic rings, the propagation constant of the fundamental and the higher-order modes of the plasmonic Bragg fiber approach asymptotically that of conventional SPPs formed at the planar interface between a semi-infinite metal and a semi-infinite dielectric medium, namely, $k_{\text{spp}} = k_0 \sqrt{\epsilon_M \epsilon_D / (\epsilon_M + \epsilon_D)}$. Although the propagation constants of the fundamental and higher-order modes deviate from the dispersion curve of k_{spp} when the number

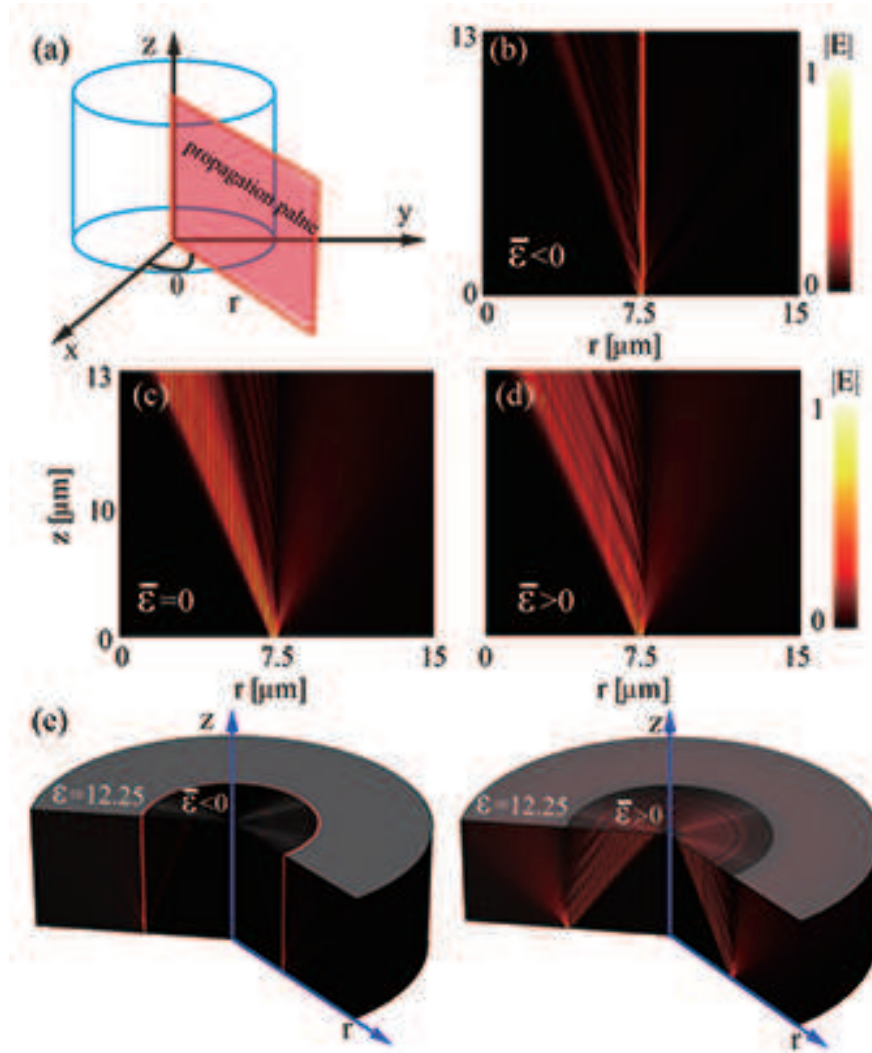


Fig. 4. Simulation of beam propagation in plasmonic Bragg fibers. The beam dynamics is shown in the radial plane, as indicated in (a). A TM-polarized Gaussian beam is injected normally at the interface between a homogeneous medium with $\epsilon_D = 12.25$ and a plasmonic Bragg fiber with negative (b), vanishing (c), and positive (d) average permittivity. The plasmonic Bragg fiber is composed of $n = 30$ dielectric-metal rings. (e) A 3D view of beam propagation corresponding to (b) and (d), respectively.

of dielectric-metal rings decreases, localized surface modes exist for any number of rings. Moreover, as shown in Fig. 3(f), when the plasmonic Bragg fiber with $\bar{\epsilon} < 0$ is replaced by a homogeneous metallic cylinder with the same radius, the radial dependence of the propagation constant of the surface modes is similar to that of the plasmonic Bragg fiber, as per Fig. 3(e). We mention here that, the imaginary part of the propagation constants of these surface modes is extremely small [$\Im m(k_z) \sim 0.003$ for all the modes shown in Fig. 3(e)], which defines an essentially long propagation length ($L_{\text{prop}} \sim 58.8 \mu\text{m}$).

Direct numerical simulations of optical beams propagating in the plasmonic Bragg fibers investigated in this work, performed by numerically solving the 3D Maxwell equations governing

the beam dynamics, corroborate the conclusions of the above analysis. Thus, Fig. 4 shows how an input TM-polarized Gaussian beam evolves in the plasmonic Bragg fiber when the operational wavelength is varied. The plasmonic Bragg fiber is composed of $n = 30$ dielectric-metal rings, and its average permittivity is tuned by varying the operational wavelength. As expected, when $\bar{\epsilon}$ of the plasmonic Bragg fiber is negative, a localized mode quickly forms at the interface between the fiber and the cladding, whereas the additional energy of the input wave diffracts off as radiation waves, see Fig. 4(b). By contrast, the input optical beam strongly diffracts without any signature of the formation of a surface mode, in the case when the plasmonic Bragg fiber has $\bar{\epsilon} = 0$ or $\bar{\epsilon} > 0$, as shown in Figs. 4(c) and 4(d), respectively.

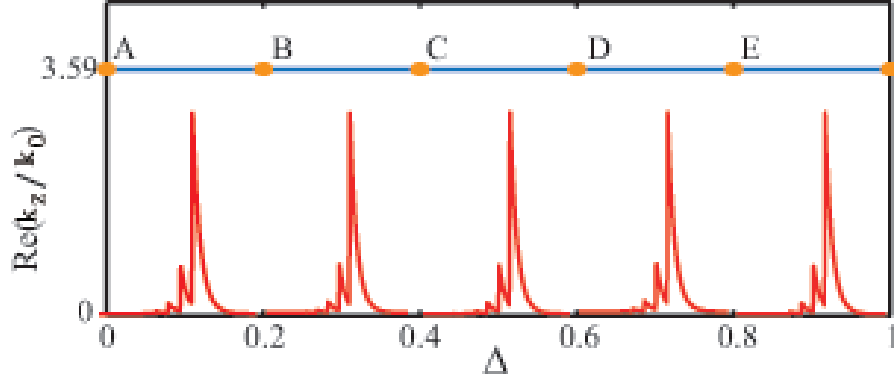


Fig. 5. The dependence of the eigenvalue (blue line) and electric field amplitude of the fundamental surface mode on the disorder level, calculated for the plasmonic Bragg fibers composed of $n = 10$ dielectric-metal rings. The operating wavelength is $\lambda = 2.2 \mu\text{m}$, thus the average permittivity of the plasmonic Bragg fiber is negative, $\bar{\epsilon} < 0$. The modal profiles are calculated for five disorder levels: 0 % (A), 20 % (B), 40 % (C), 60 % (D), 80 % (E). All results are obtained by averaging over 100 disorder realizations.

As the existence of surface modes in the plasmonic Bragg fibers is determined by the sign of the averaged permittivity, one expects that such surface modes are extremely robust against structural disorder. This is expected as a fully random structural perturbation preserves the average values of the area of the transverse cross-section of constituent cylindrical shells and thus does not modify the spatially averaged permittivity or its sign. To test this conjecture, we introduce disorder into the plasmonic Bragg fiber by assuming a random fluctuation of the area of the transverse cross-section of the metallic components. Thus, the area of the n th metallic layer is set to $\hat{S}_M^n = S_M^n + \delta_n$, where δ_n is a random value. We assume δ_n to be uniformly distributed in the interval of $[-\delta, \delta]$, $0 < \delta < S_M^1$, hence the level of disorder can be characterized by the parameter, $\Delta \equiv \delta/S_M^1$. We choose the operating wavelength $\lambda = 2.2 \mu\text{m}$ at which the unperturbed plasmonic Bragg fiber has $\bar{\epsilon} < 0$. The eigenvalues and field profiles of the fundamental surface modes determined for increasing disorder strength, Δ , are shown in Fig. 5, where the results are averaged over 100 randomly-perturbed configurations.

As recently found in planar plasmonic lattices [12], the sign of the spatial average of the permittivity determines the Zak phase of such superlattices, and the existence of interfacial modes between a superlattice with $\bar{\epsilon} < 0$ and one with $\bar{\epsilon} > 0$ can be naturally viewed as the edge modes occurring at the interface between two topologically distinct structures. For plasmonic Bragg fibers considered here, although one cannot rigorously define a Zak phase as in the case of 1D periodic structures, with the increase of the number of metallic-dielectric ring pairs, the structure increasingly resembles a 1D periodic structure as far as the outmost region is concerned. Therefore, one naturally expects that similar topological modes occur in the regions where the

average permittivity changes its sign. From this topological viewpoint, the surface modes of plasmonic Bragg fibers with $\bar{\epsilon} < 0$ are robust against structural disorder added to the photonic system. This envision is indeed confirmed by our analysis. To be more specific, as one can see in Fig. 5, the eigenvalue (propagation constant) of the surface modes is unaffected by the structural disorder, and it is actually pinned to the value of the conventional SPPs formed at the interface between a homogeneous metallic cylinder with the same radius as the Bragg fiber and a dielectric cladding. Furthermore, the spatial profile of the surface mode remains almost unchanged, even when the disorder strength increases to 80 % or even larger values. Therefore, the surface modes existing at the interface between a plasmonic Bragg fiber with $\bar{\epsilon} < 0$ and uniform dielectric cladding may be viewed as an extension of the topological modes that exist at the interface between two 1D plasmonic superlattices with opposite sign of the average permittivity.

4. Conclusion

Using both the mode analysis and direct beam propagation simulations, we have studied the surface modes of the plasmonic Bragg fibers. Our analysis has revealed that the existence of the surface modes in this setting is determined by the sign of the spatially averaged electrical permittivity. As a consequence of this property, the surface states are robust against addition of disorder to the system. The localized surface modes, which exist at the interface between the Bragg-fiber's core with $\bar{\epsilon} < 0$ and the outermost uniform dielectric medium, may be viewed as an extension of the topological modes in two 1D plasmonic superlattice with opposite signs of the averaged permittivity in the corresponding periodic sublattices. Finally, we mention that, it is known that the nonlinear optical effects are enhanced by the SPP effect, and the nonlinear change of the dielectric permittivity is even expected to change the average permittivity from negative values to positive or vice versus, which can fundamentally change the topology of the metallic-dielectric Bragg structures and consequently the condition for the existence of the surface modes. Thus it may be interesting to extend the present analysis to the light propagation in nonlinear Bragg fibers [16].

Funding

European Research Council (ERC) (ERC-2014-CoG-648328); Guangdong Natural Science Foundation (Grant Nos. 2015A030311018 and 2017A030313035); National Natural Science Foundation of China (NSFC) (61475101).